Journal of Asian Concrete Federation

journal homepage: https://jacf.sfulib3.publicknowledgeproject.org/index.php/jacf

Discrete Element Method Simulation of Aggregate Interlock Effects in Concrete with Real Rough Interfaces under Shear Loading

Zhuofan GU [a], Li WANG [a], Jiehui WANG [a,b,*], Tamon UEDA [a,*]

[a] *Colege of Civil and Transportation Engineering, Shenzhen University, Shenzhen, 518060, China*
[b] *Department of Architecture and Civil Engineaing, City University of Hong Kong, Hong Kong, China*

A B S T R A C T

It is well known that aggregate interlocking is an important contributing mechanism to the shear capacity of concrete. In this study, 3D discrete element method is employed to elucidate how aggregate interlocking affects the shear transfer and interfacial behavior of real rough concrete interfaces. Starting from a high-resolution Stereolithography (STL) model of the crack surface the roughness geometry is imported into discrete element model (DEM) as a rigid boundary while the surrounding concrete is discretized into bonded spherical particles. The shear-slip simulations show that the contact force chain is concentrated near the sharp corner peaks, producing localized dilatation and progressive microcracks. Simulation of experimental displacement-load curves, where the peak shear strength increases nearly linearly to a critical value beyond which particle fragmentation at the surface limits further increases, provides an explanation for the aggregate damage phenomena observed in the pushover tests. By tracking bond fracture and slip localization, the model provides interpretable evidence to explain the interfacial shear resistance of recycled aggregate concrete (RAC) and natural aggregate concrete (NAC). It demonstrates the applicability of discrete element model for real rough interface in numerical simulations of aggregate interlock. It also highlights the differences in DEM results between RAC and NAC, which reflect shear-slip through real rough interfaces.

Keywords: DEM, Aggregate interlock, Real interface, Shear transfer

1. Introduction

Concrete is a relatively brittle material that is prone to cracking under tensile stress. The feature of brittleness is more complex than with other brittle materials because concrete exhibits more quasi-brittle material properties, which partly come from the heterogeneity characteristics of concrete. Shear transfer in cracked concrete has traditionally been attributed to the anchoring force of the reinforcement, the residual cohesion of the cement matrix, and aggregate interlock. Aggregate interlock is activated when two crack surfaces slide and expand relative to each other. Therefore, the reasonable design requires a comprehensive understanding of fracture mechanics, post-cracking strain, and stress transfer. As such, aggregate interlock is a central element of shear friction provisions in modern design codes and analytical models ranging from Walraven's two-phase concept [1] to Bazant's rough crack theory [18, 19]. Over the past few decades, different models have been developed to calculate the aggregate interlock capacity of concrete. Examples include Walraven's simplified formulae [1] and Cavagnis's aggregate interlock formulae [2]. However, there is less evidence in the literature that the stresses and interface behavior of real crack interfaces can be simulated.

Numerical simulations offer a complementary perspective for elucidating these mechanisms. In order to develop the theoretical model of aggregate interlock, it is necessary to develop the real crack surface of concrete. Therefore, it is not practical to treat concrete as a homogeneous and continuous medium because it does not represent the real contact and stress transfer of the roughness of the crack and the crack interface.

The progress and shortcomings of existing research from two perspectives, aggregate interlock models in cracked

*Corresponding author: Jiehui WANG (jiehwang@cityu.edu.hk), Tamon UEDA (ueda@szu.edu.cn)

DOI http://dx.doi.org/10.18702/acf.2026.12.1.33

Received: 04-Nov-2025; Revsed: 20-Jan-2026; Accepted: 21-Jan-2026; Published online:31-March-2026

ISSN 2465-7964, eISSN 2465-7972.

concrete and numerical simulation in cracked concrete, are analyzed, and the research gap is consequently identified in the following section.

1.1 Overview of aggregate interlock models in cracked concrete

Walraven [1] developed the empirical equation for aggregate interlocking based on the experiment using push-off specimens with externally restrained reinforcement. His equation includes two relationships between four variables (i.e., shear stress, shear displacement, normal stress, and opening displacement). Cavagnis et al [2] developed an analytical formulation based on Walraven's two-phase model that takes into account the path of crack motion and is more representative of the actual situation. However, it should also be noted that the Cavagnis equation takes into account the effect of the residual tensile strength of concrete on the normal stresses generated by aggregate interlocking [2]. under various stress paths such as monotonic and cyclic loading [3,4]. The model assumes that the cracked surface is a set of contact cells with various inclinations, and the distribution of the inclinations of the contact cells is called the contact density function, which is the core of the model proposed by Li, Maekawa et al [3]. The geometry of the cracked surface is assumed to be characterized by infinitesimal contact cells. The model proposes a contact density function that represents all possible contact units as well as possible contact areas and orientations. Then, for the monotonic loading of push-off experiments, the total stress transmitted by the contact units can be obtained by an integral operation on the contact density function.

1.2 Review of numerical simulation in cracked concrete

Finite element methods (FEM) equipped with cohesive-zone or embedded-crack formulations have been used with success to simulate mixed-mode fracture. Thushara [5] develops a two-step meso-scale finite element framework that first lets a concrete prism crack in uniaxial tension and then re-uses the fractured geometry to quantify aggregate interlock shear transfer. while applying the finite element method to simulate cracked concrete, the key issues mainly focus on the following aspects (Table 1). (1) Aggregate shape generation, distribution, and overlap check (2) Insertion of zero-thickness cohesive units. Zero-thickness cohesive units can be inserted into the finite element mesh in two different ways: (I) the pre-insertion method, also known as the intrinsic cohesion method [6], and (II) the dynamic insertion method during analysis, also known as the extrinsic cohesion method [7]. Cohesive interface elements are widely used in numerical simulations to model fracture and interfacial behavior in concrete and concrete-based composites. These elements, often based on cohesive zone models, allow for realistic simulation of crack initiation and propagation under various loading conditions, such as bending or tension, by capturing the nonlinear mechanical response at interfaces within the material or between different materials like steel and concrete. At the mesoscale, cohesive interface elements have been integrated into models of fiber-reinforced concrete, enabling accurate prediction of both matrix cracking and the influence of fibers on fracture processes, with numerical results closely matching experimental tests [8]. Additionally, cohesive interface elements have been applied to simulate the interfacial slip and shear behavior in steel-concrete composite structures, offering an efficient alternative to labor-intensive push-out tests and successfully capturing the nonlinear slip and stress distribution at the interface [9]. In addition, cracked concrete requires additional steps and methods to handle fracture elements and meshes between simulated crack models [5]. Based on physical crack generation, geometric recovery, simplified contact treatment, and other methods, the finite element model is simplified and accurate. The modeling process for the entire FEM study is shown in Table 1 and Figure 1.

Table 1 Flowchart of the proposed FE approach for aggregate interlock using fractured mesoscale models [5]

Modeling sequence	Method
1	Generate aggregates in MATLAB and transfer aggregates to ABAQUS (Figure 1 (a))
2	Develop the mesoscale model in Abaqus and mesh using tetrahedral elements
3	Create the input file
4	Insert cohesive elements to the input file using cohesive elements generator
5	Import the input file to Abaqus as a model and check the model
6	Run the model until discrete crack propagate between notches (Figure 1 (b))
7	Open a new model and import the .obd file as a part
8	Delete the cohesive elements ranging between two crack surfaces
9	Separate the two cracked halves and export them one by one as a .stl file
10	Import each .stl files to BLENDER
11	Use weld function to the remove cohesive elements inside
12	Export the model as .stl file and import it back to Abaqus
13	Create the geometry using "create geometry using mesh" plugin (Figure 1 (b))
14	Use virtual topology to remove mesh details on the geometry
15	Insert the material properties, contact Definition and boundary conditions for aggregate interlock analysis (Figure 1 (c))

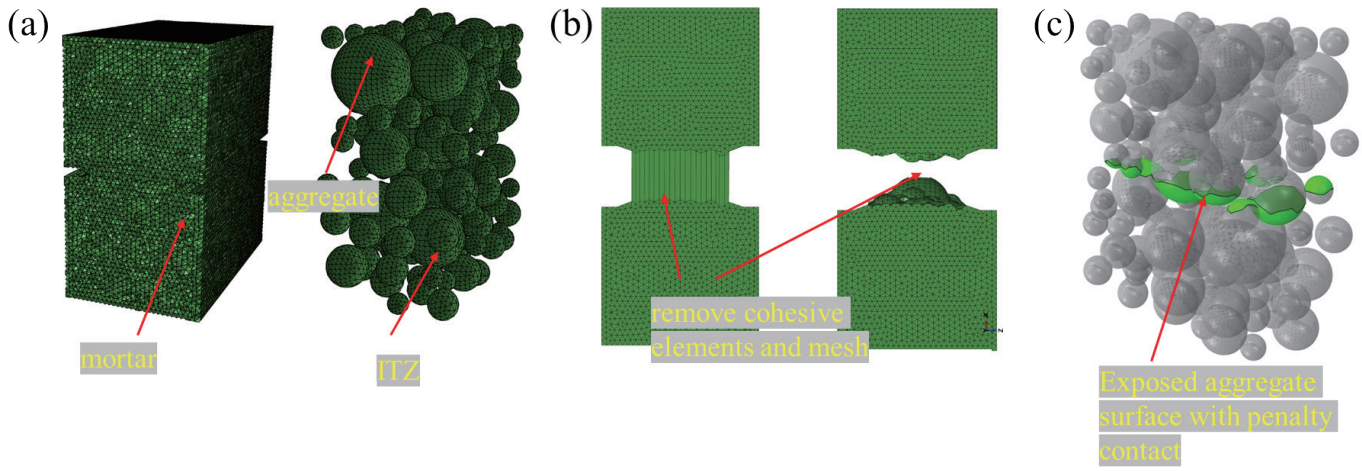

Figure 1 FEM for aggregate interlock mesoscale models: (a) mortar, aggregate, and ITZ for the model, (b) remove cohesive elements and meshes between surfaces, and (c) contact between aggregate interlock elements [5]

By contrast, discrete element method (DEM) represents concrete as a disordered packing of rigid grains linked by breakable bonds. The bonded-particle model introduced by Potyondy et al. extends classical contact mechanics with bonds that can fail in tension, shear or bending [10, 11]. Although DEM, especially when implemented through particle flow codes (PFC), has become a powerful tool for simulating complex mechanical behavior, fracture processes, and microstructural phenomena in concrete and cementitious materials, its application in fracture shear problems in concrete remains in its infancy. The PFC series of software, based on the explicit DEM, provides an ideal platform for simulating aggregate interactions, as it can model the loading, rotation, and failure processes of individual particles, bonding, and contact, thereby revealing the progressive failure mechanisms of concrete interfaces. Most DEM simulations focus on various concrete types, including fiber-reinforced concrete, permeable concrete, and self-compacting concrete, as well as phenomena such as crack initiation, propagation, and the influence of aggregate morphology and the interfacial transition zone (ITZ) [12, 13, 14, 15, 16, 17]. DEM simulation of interface behavior is mainly concentrated in the fields of rock mechanics and concrete-rock contact. These studies have two limitations: (1) idealized cylindrical or prismatic specimens with artificially serrated interfaces; (2) studies rely on synthetic roughness rather than the actual fracture geometry of laboratory specimens. Therefore, shear simulation studies of real rough interfaces remain under-explored.

Most DEM studies adopt a mesoscale description, treating concrete as a composite material consisting of mortar, coarse aggregate, and the ITZ. For example, Nitka and Tejchman [26] conducted experimental studies on crack formation and propagation using acoustic emission and digital image correlation techniques, and then compared the experimental results with numerical analysis results. Nitka and Tejchman [32] also used mesoscale DEM simulations based on two-dimensional X-ray scans to simulate the complex fracture process of reinforced concrete short beams. Despite the simplification of the two-dimensional conditions, the DEM analysis and internal laboratory tests achieved a good level of consistency in terms of vertical forces as a function of deflection and the evolution of failure mechanisms. Zhou et al. [27] demonstrated that microcracks appeared in the specimens before reaching peak load and failure. Using the Flat-Joint model in discrete element method software, two contact models were established. The results of this study indicate that the established discrete element model can accurately simulate the stress field. Yu et al. [28] addressed the strain rate-dependent dynamic behavior of concrete structures by proposing a multi-scale modeling method for concrete structural dynamic response that combines macro-scale FEM with meso-scale DEM. Using the macro-scale finite element method with representative volume elements, the micro-scale discrete elements composed of aggregates, mortar, and interfaces were used to simulate the strain rate effects of concrete. Zhao et al. [29, 30] developed an advanced discrete element model that accurately describes the microstructure of concrete, including different interface transition zones, random adhesive mortar distribution, and non-uniform material properties. Zhang et al. [31] investigated the dynamic shear properties of the sand-irregular concrete interface by conducting a series of direct shear tests under dynamic normal loads. The tests were designed with different interface roughness coefficients. The results indicated that larger dynamic normal load amplitudes and frequencies cause changes in the micro-mechanical behavior of concrete.

1.3 Research objectives and highlights

The use of the DEM to investigate stress transfer and interface behavior in cracked concrete is primarily advantageous due to its ability to explicitly model contact surfaces and calibrate appropriate micro-parameters based on compressive strength, tensile cracking strength, and fracture energy. To conduct a more realistic, simplified, and more convenient numerical simulation of aggregate interlock, this study models concrete at the mesoscale level using the DEM to represent the concrete mass element, with real interface

data imported into the model to define the contact between the two sides of the element. Building on this capability, this study aims to develop a type of discrete element modeling method to use concrete mesoscale models to study stress transfer and interface behavior caused by aggregate interlock. The differences between mesoscale models of normal aggregate concrete (NAC) and recycled aggregate concrete (RAC) fracture were evaluated based on real rough interfaces. Finally, the advantages and disadvantages of the developed DEM method are discussed, and further research directions for aggregate interlock models are suggested.

2.Materials and Methodology

This study introduces an innovative approach of incorporating real rough interfaces into 3D discrete models to simulate the aggregate interlock mechanism of cracked concrete. In DEM, interface behavior is governed by the contact models between particles. Real concrete crack interfaces typically exhibit complex roughness and irregular interlocking morphologies, which determine the distribution and orientation of local particle contacts. Importing the actual interface profile into the particle contact definition ensures that the geometric conditions of the interface in the simulation are consistent with those of the physical specimen, thereby preserving the fundamental geometric features of aggregate interlock and surface roughness. Under constant normal stiffness conditions, it examines the effects of concrete strength and aggregate type variables on interface aggregate interlock. Based on the results of numerical simulation, it analyzes the effectiveness of discrete element simulation of real interfaces, the reproducibility of NAC and RAC shear tests, the real interface behavior and crack extension phenome on 3D interfaces.

2.1 Concrete property test

The mix design for NAC and RAC is presented in Table 2. The RAC was proportioned to be nominally equivalent to NAC, with the same target binder content, aggregate gradation, and water-cement ratio. To achieve equivalent proportions, the volume of coarse aggregate was maintained approximately constant between NAC and RAC mixes. Moreover, the aggregate sizes of NAC and RAC are roughly the same (Figure 3).

For the aggregate interlock experiments, cubic specimens with dimensions of 150 × 150 × 150 mm were prepared. The experimental setup consists of the restraint fixture and the uniaxial electro-hydraulic servo loading system, which can simultaneously apply vertical loads and collect horizontal restraint stresses in parallel, as shown in Figure 2 (a). And these grooves defined a central test interface area of approximately 150 × 105 mm (Figure 2 (b)). Pre-cracking and splitting were induced by inserting a steel wedge into the grooves, as illustrated in Figure 2 (b). This procedure was designed to promote controlled crack formation along the intended plane while minimizing unwanted crushing or secondary cracking. By creating a single, well-defined fracture interface.

Table 2 Concrete experiment mix design

		NAC-30	NAC-60	RAC-30	RAC-60
Natural aggregate	kg	1031	1073	0	0
Recycled aggregate	kg	0	0	1031	1073
Fine aggregate	kg	778	603	778	603
Cement	kg	382	550	382	550
Water	kg	195	165	195	165
Additional water	kg	0	0	31	32
Water-cement ratio		0.51	0.30	0.51	0.30
Superplasticizer	kg	0.382	0.55	0.382	0.55
Slump	mm	9.5	6.5	9.7	8.8
Fc (CoV)	MPa	30.6 (3%)	60.2 (1%)	28.7 (4%)	49.9 (5%)

2.2 Obtaining and processing real interface STL files

This study firstly proposes an innovative approach that includes importing STL files containing real interface data into the model. Regarding obtaining STL files, the study used KEYENCE’ s profile scanning machine (VR-5000) to laser scan the interface of cracked concrete, generating a 105×150mm interface profile, and then exported the STL file using analysis software (Figure 4 (a) and (b)). Owing to the high precision of the scanning (0.001 mm), subtle interface defects and numerous surface fragments could be clearly identified on medium-sized concrete interfaces. To ensure the stability and computational efficiency of consequent numerical modeling, interface processing software to reconstruct the scanned geometry and repair for the noise in the scanned data, followed by the generation of a sparse triangular mesh (Figure 5 (a) and (b)). However, reconstruct and repair is necessary Because the interface obtained through the initial profile scan is quite precise, the STL file consists of millions of triangular patches (Figure 5 (a)) and the profile measured by non-contact laser reflection may have some local defects due to the laser reflection path being blocked. Finally, the processed interface will be imported into the DEM model to define the contact on both sides of the interface.

the aggregate. This allows for the insertion of zero-thickness cohesive elements with 6 nodes (COH3D6) at the interface, as schematically depicted in Fig. 4. For the FRP-confined concrete specimens, the FRP jacket is meshed using 4-node quadrilateral shell elements with reduced integration (S4R) and is tied to the surface of the concrete cylinder. The

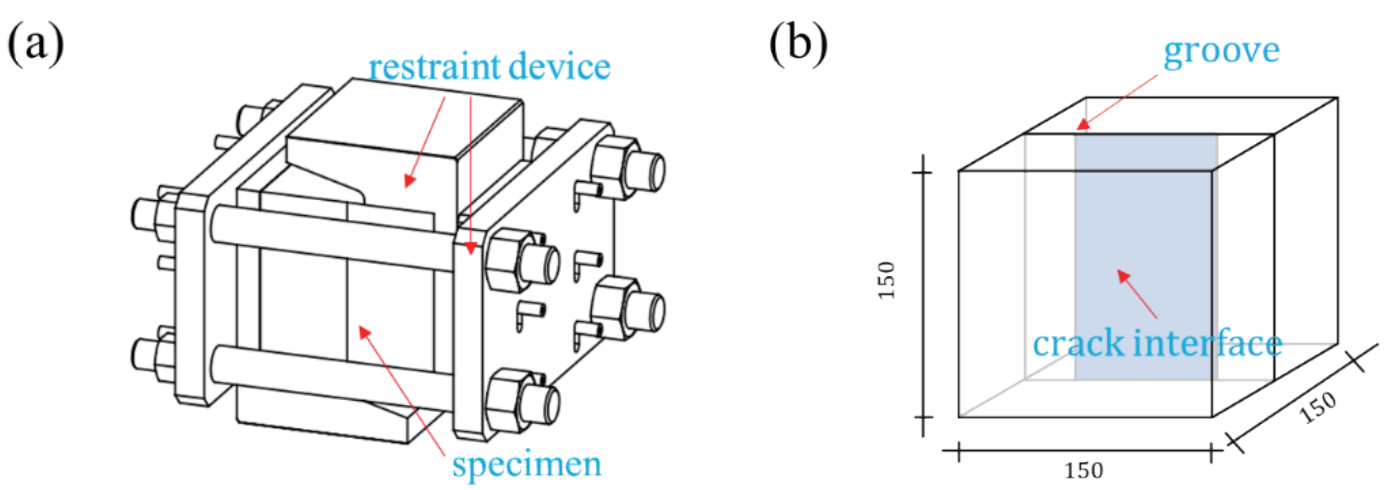

Figure 2 Experiment device and specimen diagram

elastic modulus of GFRP and CFRP in the hoop direction are 81300 MPa and 250000 MPa, respectively, which are obtained from flat coupon tensile tests. The nominal thicknesses of a single ply of GFRP and CFRP sheets are 0.170 mm/ply and 0.111 mm/ply, respectively. In the model, the elastic modulus in the axial direction, Poisson's ratio, and shear modulus of the FRP are deliberately set to zero to eliminate the biaxial effect of the confining material [27][28].

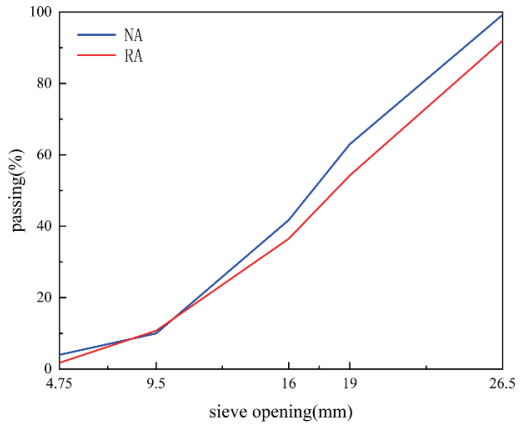

Figure 3 Aggregate particle size distribution

2.3 Numerical model establishment

The model dimensions are set to a cube size of 150 × 150 × 150 mm. Additionally, the real interface of 105 × 150 mm must be set in the center of the model. Therefore, it is necessary to set grooves on both sides of the long side of the interface so that the discrete elements on both sides do not contact each other. Figure 6 (a) and (b) presents the specific model construction setup, with detailed procedures provided as follows.

1) The first step is to generate particles. Generate uniformly distributed particles in the model. Specifically, the particles are densified on both sides of the model (around the interface) to ensure that the contact defined by the interface is fully filled, and to ensure the stability and accuracy of the calculation and meet the computing power of the computer.
2) The second step is to bond. It defines the upper and lower particles at the interface as the Linear Parallel Bond Model, and it sets the parameters for the particles. A detailed introduction to the Linear Parallel Bond Model is provided in section 2.3.1.
3) The third step is to create structural surfaces. The study imports the real interface profile into the defined particle contact. It changes the contact mode defined by the interface to the Smooth-Joint model. The Smooth-Joint Model simulates the behavior of a plane interface under expansion conditions, regardless of the direction of local particle contact along the interface. It simulates the behavior of a friction joint by assigning the Smooth-Joint Model to all contact points between particles on both sides of the interface. This method ensures that the Smooth-Joint Model is always present at the joint surface contact during shearing. Otherwise, the accuracy and reliability of the model may be affected, resulting in errors in the simulated shear strength as the shear displacement increases. A detailed introduction to the Smooth-Joint Mode Model is provided in section 2.3.2.
4) The fourth step is to create walls, which represents the displacement constraint in the experiment. Use the Wall command to generate a shear box for shear-slip simulation, and there is no friction between the wall and the particles.
5) The fifth step is to define constraints. Write the constraint conditions for the servo mechanism using the Fish language (FISH is an embedded programming language that enables users to interact with PFC models and create PFC models, defining new variables and functions as needed. These features can be used to extend the practicality of PFC or add user-defined features. For example, a particle model can be applied to servo control to perform numerical tests.) to control the preload of

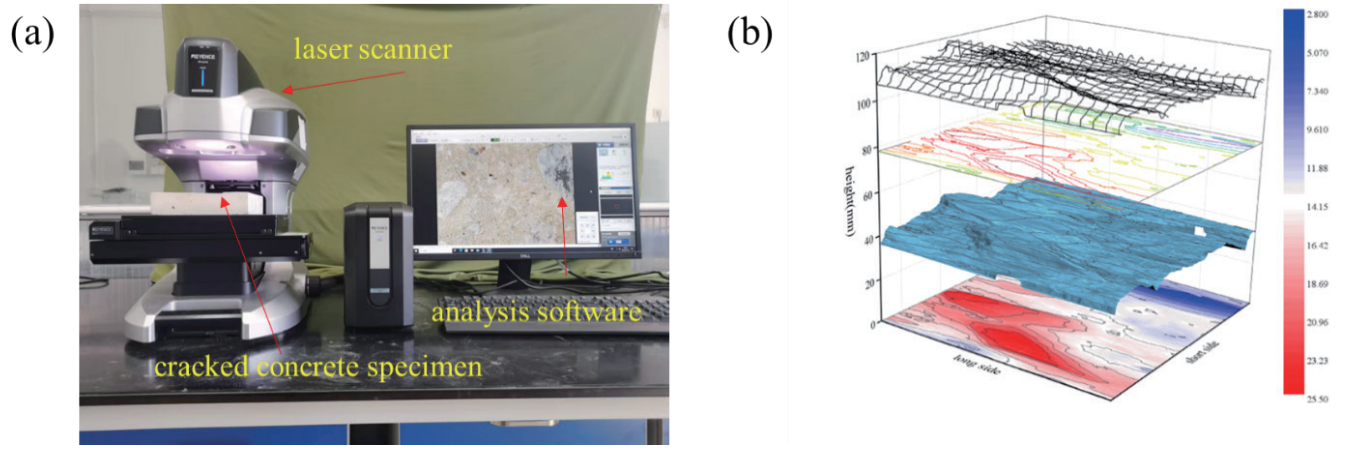

Figure 4 Interface profile measurement: (a) profile scanning, and (b) rough interface profile image

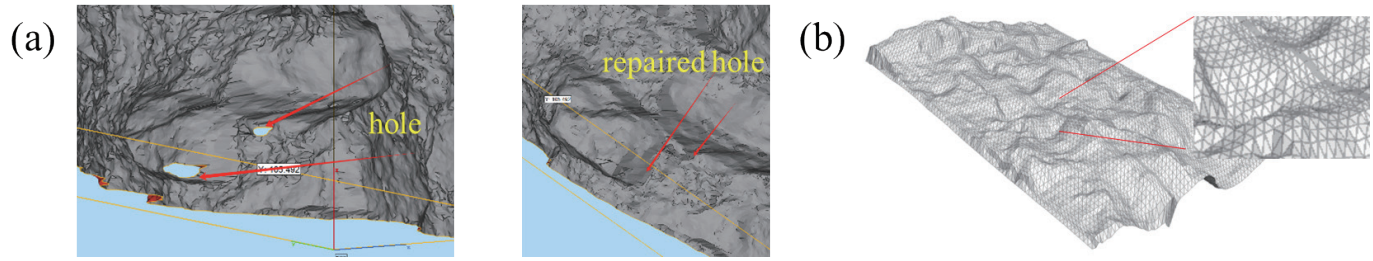

Figure 5 STL file processing: (a) interface repair, and (b) import interface profile overview

the normal force. Next, add the initial conditions for the preload, which mainly simulate the residual stress that typically exists in cracked concrete before the shear-slip. The constant constraint stiffness of the initial conditions is achieved by turning off the servo mechanism during the simulation and then using the wall constraints.

6) The sixth step is to load. The maximum shear displacement in the simulation settings is 7 mm, and quasi-static loading conditions are used. It outputs the calculation results at different displacement positions for comparative analysis.

2.3.1 Linear Parallel Bond Model

To minimize the error between numerical simulation models and indoor test results, a more appropriate contact model should be selected. This model should not only better reflect the test results but also consider its feasibility. The parallel key contact model proposed by Potyondy and Cundall [23] meets the above requirements (as shown in Figure 7). This model requires fewer parameters and can effectively simulate the upper and lower concrete shear-sliding bases. A parallel bond provides the mechanical behavior of a finite-sized piece of cement-like material deposited between the two contacting pieces. The parallel-bond component acts in parallel with the linear component and establishes an elastic interaction between the pieces. Parallel bonds can transmit both force and moment between the pieces [20].

Assuming that the particles on both sides have constant stiffness (tangential and normal) and that the contact point is the center of both particles, the particles can rotate freely in different directions (tangential and normal). Rotation can generate torque between the particles, while contact bonding only transmits force and does not resist force. Parallel bonding not only transmits force but also transmits torque. The linear parallel bond model provides the behavior of two interfaces: an infinitesimal, linear elastic (no-tension), and frictional interface that carries a force and a finite-size, linear elastic, and bonded interface that carries a force and moment (see Figure 7) [21, 22, 23].

Given that particles are discrete and discontinuous, the mechanical properties of concrete cannot be directly assigned to individual particles. Therefore, numerical simulations of shear-slip tests are typically based on laboratory-measured mechanical properties of concrete, and relevant numerical simulation mechanical tests are used to calibrate the various micro-scale parameters required for the shear test model. The results of the simulated mechanical tests are in good agreement with those of the laboratory tests, and these parameters can be used to simulate the actual shear mechanical behavior and failure patterns.

2.3.2 Smooth-Joint Model

The Smooth-Joint model simulates the behavior of a planar interface with dilation regardless of the local particle contact orientations along the interface (Figure 8) [21,22,24]. The behavior of a frictional or bonded joint can be modeled by assigning smooth-joint models to all contacts between particles that lie on opposite sides of the joint [24]. This feature will be very useful for showing the failure and reconstruction

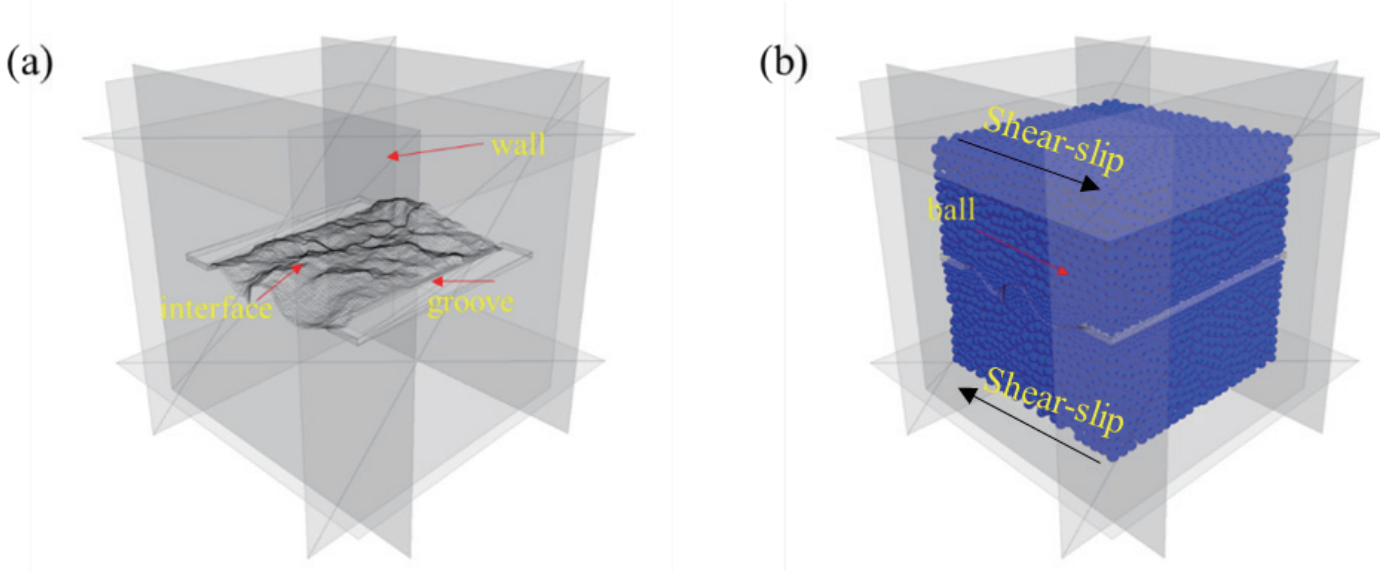

Figure 6 Real interface discrete element model: (a) boundary constraint and real interface, and (b) overall model

of interlock units at concrete interfaces under shear-slip conditions. This is because interlock units at the interface will form new interlocks with the failed interface under constraint after failure. The behavior of the bonded interface is linear elastic until the strength limit is exceeded and the bond breaks, making the interface unbonded; the behavior of an unbonded interface is linear elastic and frictional with dilation, with slip accommodated by imposing a Coulomb limit on the shear force. The interface does not resist relative rotation (Figure 8). If in small-strain mode, a contact with the Smooth-Joint model is always active. In this mode, the contact will never be deleted. If in large-strain mode, a contact with the Smooth-Joint model is active if the contact is bonded or if the contact gap is negative or the two pieces are overlapping (Figure 9).

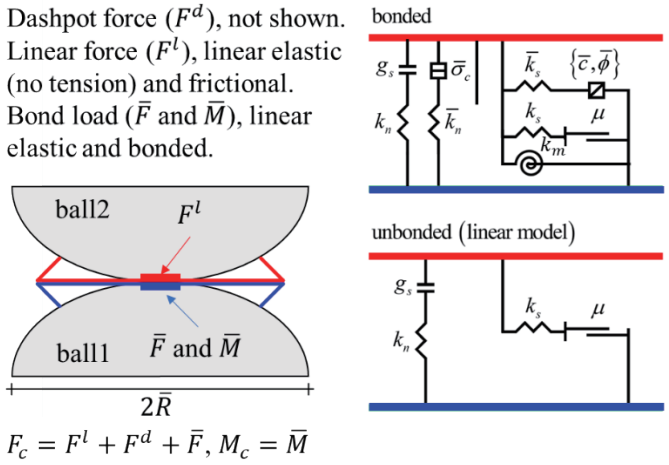

Figure 7 Behavior and rheological components of the linear parallel bond model with inactive dashpots [21, 22, 23] (Linear Model: k_n : normal stiffness, k_s : shear stiffness, k_m : rotation stiffness, μ : friction coefficient, g_c : reference gap

Parallel-Bond Model: $\bar{k}_n$: normal stiffness, $\bar{k}_s$: shear stiffness, $\bar{\sigma}_c$: tensile strength, $\bar{c}$: cohesion, $\bar{\phi}$: friction angle)

2.4 Numerical calculation scheme

To investigate the shear behavior of cracked concrete interfaces under different material and geometric conditions, a series of DEM simulations was performed. The simulations were designed to systematically evaluate the influence of concrete strength, aggregate type, and realistic interface geometry on the predicted mechanical response. Given that particles are discrete and discontinuous, the mechanical properties of concrete cannot be directly assigned to individual particles. Therefore, numerical simulations of shear-slip tests are typically based on laboratory-measured mechanical properties of concrete, and relevant numerical simulation mechanical tests are used to calibrate the various micro-scale parameters required for the shear test model [39, 40]. The results of the simulated mechanical tests are in good agreement with those of the laboratory tests, and these parameters can be used to simulate the actual shear mechanical behavior and failure patterns. Specific parameters are listed in Table 3. Thus, the numerical scheme was systematically designed as follow:

1) The influence of concrete strength on numerical simulation calculation to examine how variations in compressive strength influence the predicted shear response and failure behavior in the DEM model.
2) The influence of concrete type (aggregate type) on numerical simulation calculation to analyze the impact of using different aggregate types, such as natural aggregate and recycled aggregate, on interface mechanics and shear resistance
3) Numerical model calculation of different real interfaces to discuss interfaces reconstructed from high-resolution scans to study how realistic surface morphology affects shear performance.
4) Analyze the DEM of real rough interfaces to simulate the effect of aggregate interlock and the mechanism of aggregate interlock.aggregate interlock.

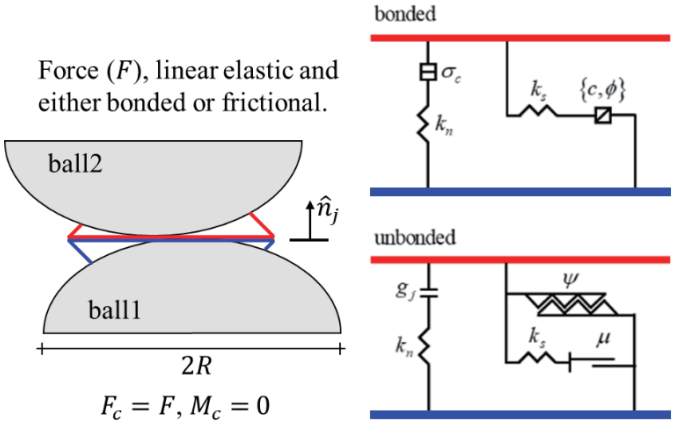

Figure 8 Behavior and rheological components of the Smooth-Joint model
(Smooth-Joint Model: k_n : normal stiffness k_s : shear stiffness c: cohesion ϕ : joint friction angle σ_c : tensile strength μ : friction coefficient g_j : joint gap Ψ : dilation angle)

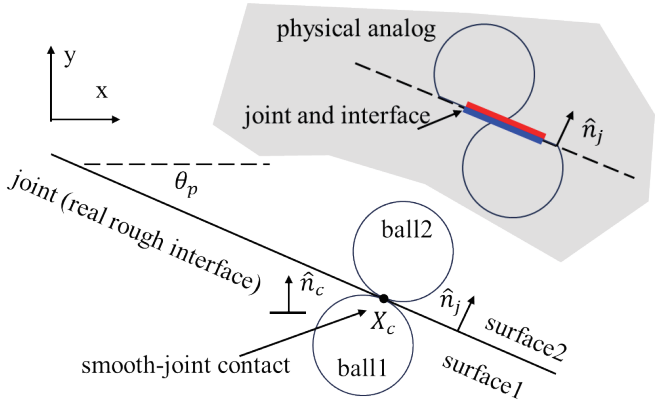

Figure 9 Joint (real rough interface) and Smooth-Joint contact

The maximum shear displacement was set as 7 mm, and the real interface data was obtained from the contour scan of the test section. The loading rate was set to quasi-static loading conditions [40]. However, since PFC uses meters per second (m/s) as the default speed unit, the nominal value does not directly correspond to the actual experimental loading speed. A loading speed of 1.0 m/s was adopted, which is sufficient to simulate quasi-static loading conditions. When the load speed is 1.0 m/s, it takes approximately several hundred computational steps to produce a shear displacement of 1 mm, which is a relatively slow shear rate. For this condition, it is considered acceptable to simulate quasi-static shear-slip.

3.Numerical simulation results and reliability

3.1 Comparison of DEM crack and interface morphology with experiment

This section verifies and compares the real rough interface with the profile defining contact in the DEM. Undoubtedly, as we previously discussed about the interface treatment, this will generate differences between them. However, at the mesoscale we are studying (the minimum particle filling size in the DEM), this difference is acceptable. As shown in Figure 10 (a), the interfaces on both sides of the comparison are consistent in peak and valley profiles and maintain uniformity in overall contour height variations. In two dimensions (Figure 10 (b)), comparing the rough contour curves on the interfaces also confirms that the variations are largely consistent, whether for real rough interfaces or those in the DEM. Within the range of DEM particle sizes, defining contact interfaces can satisfy the geometric characteristics of real rough interfaces. The consistency of peak and valley structures with the profile sufficiently reflects real rough interface contact issues, thereby further satisfy subsequent DEM result analysis.

Table 3 Micro-mechanical parameters of the DEM for real rough interface

Parameter Type	Parameter (unit)	Value
Basic Physical Parameters	density (kg/m^3)	2770
	minimum particle size radius (mm)	1.4
	particle modulus (Pa)	45e9
Contact Model Parameters	stiffness ratio: kn/ks and $\bar{k}_n/\bar{k}_s$	1
	friction coefficient	0.52

3.2 Comparison of DEM cracks with experiment

This section assesses the fidelity of the DEM model by comparing simulated crack patterns with laboratory observations for the same specimens, both before and after shear-slip (The real rough interface of this DEM originates from the interface after shear-slip test.). For sample, the experimental photographs (top) are paired with corresponding DEM outputs (bottom) on the two opposite faces: Figure 11 (a) and (b) show the before shear-slip condition, while Figure 11 (c) and (d) show the after shear-slip condition. The comparison focuses on key descriptors of fracture behavior: (1) crack initiation, (2) crack evolution, and (3) signs of dilation and local crushing and spalling. Agreement across these features provides validation that the calibrated bonded-particle model and interface treatment capture the dominant mechanisms governing aggregate interlock driven cracking, whereas model discrepancies (overly smooth paths) indicate model limitations and guide refinements. The detailed observations are discussed below.

3.3 Comparison of numerical simulation results with experiments

To verify the DEM results, shear tests corresponding to real rough interfaces are considered. Significantly, the verification of the simulation results is based only on the corresponding

shear-slip curves, which is determined by the identical initial conditions between the tests and the simulation. According to the DEM analysis results shown in Figure 12, although the simulation of the real interface is complex, the DEM still achieves considerable accuracy. In fact, the DEM well captures the simulation of shear stress and shear slip. Only the peak shear stress of aggregate interlock is slightly underestimated, which is explained by the difference between the mesoscopic scale of aggregate interlock and the DEM. Furthermore, the study also focuses on localized compaction at the interface contact region to better achieve mesoscale contact.

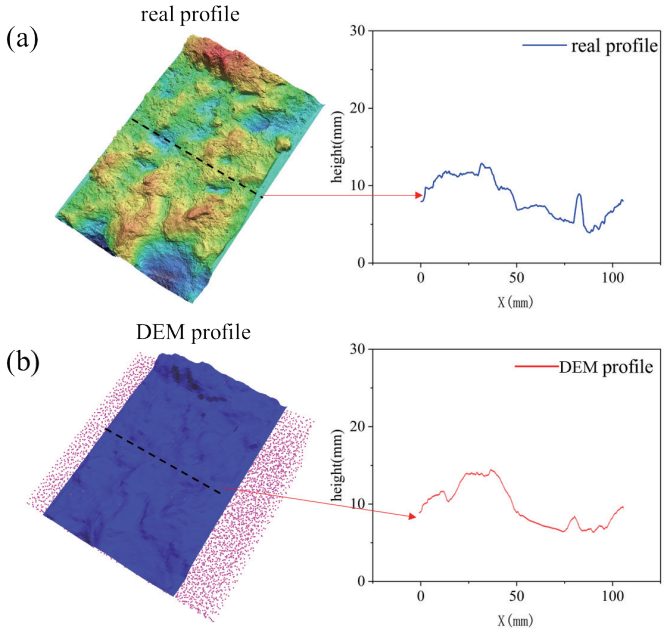

Figure 10 Comparison of real profile and DEM profile: (a) three-dimensional profile,

As shown in Figure 12, compared with the experimental curve, the DEM results have a certain degree of accuracy in the initial region before reaching the maximum shear stress. However, when the peak shear stress of aggregate interlock is reached, the DEM results deviate from the experimental curve and underestimate the peak shear stress (10.4%-16.2%). The slight underestimation of peak shear strength in the DEM simulations can be attributed to several inherent modeling idealizations. Simplified particle shapes and contact geometries approximate, but do not fully capture, real aggregate angularity and interlock, thereby reducing local stress concentration and mechanical interlocking effects. The adopted contact and bond models—calibrated primarily to match global compression–tension behavior—may also provide lower shear stiffness or strength than actual aggregate–mortar interfaces, making shear capacity more sensitive to micro-parameter choices. Additionally, the selected particle size distribution, used as a compromise for computational efficiency, limits the resolution of small-scale interlock and force-chain development. Finally, the absence of particle crushing or fragmentation mechanisms prevents the model from capturing shape evolution and local failure processes that may influence the peak shear response. In the post-peak numerical representation, the DEM results better reflect the role of interface particles in providing support and stress transfer in localized regions even after failure. Therefore, the curve exhibits a post-peak rise or smooth segment. The reason lies in the Smooth-Joint Model defining crack interface contact, whose characteristics ensure the model maintains and redistributes during shear-slip processes. This feature is similar to the failure and reconstruction of contact elements at concrete interfaces during shear-slip processes.

3.4 The Influence of Concrete Strength on aggregate interlock

Based on the shear stress-slip curves provided, concrete strength exerts a substantial impact on aggregate interlock behavior. Figure 12 (a) and (b) clearly demonstrates that higher strength concrete (NAC60) achieves significantly higher peak shear stresses compared to lower strength concrete (NAC30), suggesting enhanced aggregate interlocking capability at increased concrete strengths. This distinction indicates a strength-dependent aggregate interlocking performance, where higher concrete strength provides stronger resistance against aggregate slippage and degradation. Thus, concrete strength directly correlates to peak shear capacity, with higher-strength concretes exhibiting superior aggregate interlocking performance. Furthermore, the experimental curves (E) generally rise more steeply and reach higher peak stresses compared to simulation curves (S). As shown in Figure 10, as concrete strength increases, the slope of the first stage for NAC60 and RAC60 is greater than that for NAC30 and RAC30. This phenomenon is observed in both experiments and simulations. Under the same strength conditions, the slope of the experimental curve rises linearly to the peak strength in the first stage; however, the simulation exhibits a significant decrease in slope due to interface softening before reaching the peak strength. This phenomenon reflects that in the experiment, the destruction of the contact interface will be followed by shear-slip to reconstitute a new contact structure between the interface and the particles; for the simulation, the failure of the particles on the contact interface leads to the failure of the DEM link. In addition, the smaller-scale internal locking of the experimental interface is ignored in the DEM.

3.5 Influence of concrete type (aggregate type) on aggregate interlock

The shear stress-slip curves illustrate the significant effects of aggregate type on aggregate interlock. Comparing natural aggregate concrete and recycled aggregate concrete, the NAC specimens (Figure 12 (a) and (b)) consistently demonstrate higher peak shear stresses and more pronounced post-peak declines, indicating stronger aggregate interlock performance attributed to the strength and integrity of natural aggregates. In contrast, RAC specimens (Figure 12 (c) and (d)) exhibit lower peak shear stresses and more gradual, flattened post-peak responses, suggesting weaker aggregate interlocking due to premature fracture and degradation of recycled aggregates. Moreover, the differences between experimental

and simulation results in RAC are comparatively smaller, reflecting the diminished but more predictable aggregate interlock behavior. Thus, aggregate type is pivotal, with natural aggregates distinctly enhancing shear resistance and interlock efficiency relative to recycled aggregates.

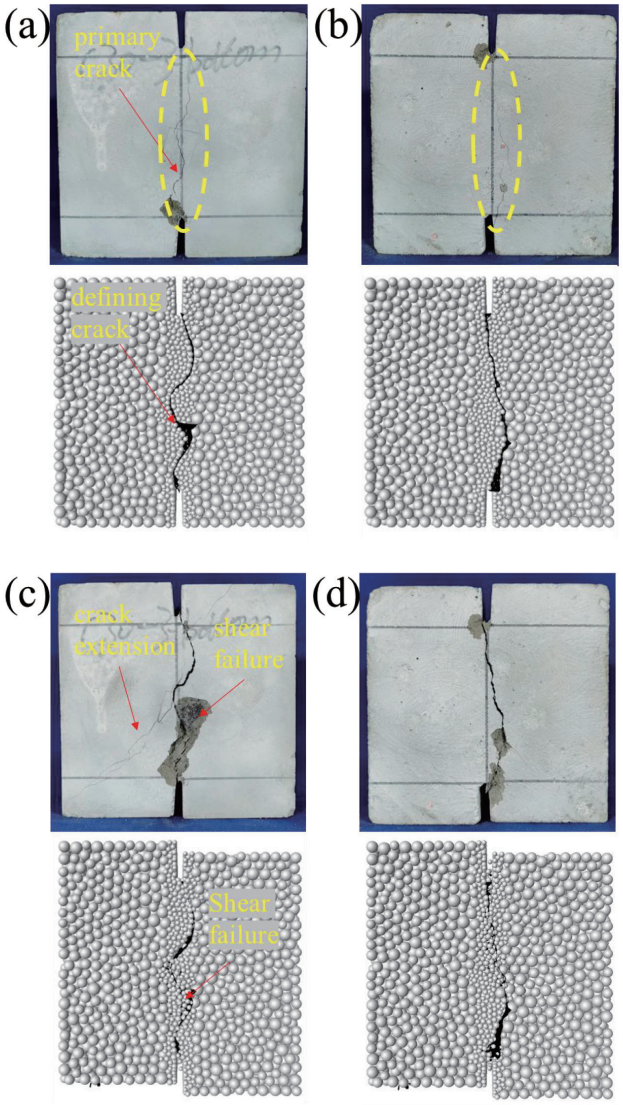

Figure 11 Comparison of cracks between experiments and DEM: (a) and (b) crack morphology on the front and back sides of the specimen before shear-slip, (c) and (d) crack morphology on the front and back sides of the specimen after shear-slip

3.6 Influence of different real interfaces before and after shear-slip on aggregate interlock

There are two types of real rough interfaces in the experiment. The first is the "complete" interface after the split test, and the second is the "damaged interface" after the shear-slip test. Based on the provided shear stress-slip curves (Figure 13), the differences between the interfaces on the two sides of the same crack are clearly evident. Figure 13 (a), representing the shear-slip interface, shows two simulation curves with distinct peak shear stresses and post-peak behaviors. The red curve (NAC30-2-S) demonstrates a higher peak shear stress and more prolonged shear resistance than the blue curve (NAC30-1-S), indicating that even within the same crack, initial fracture creates significantly different roughness characteristics on opposing interfaces (Figure 15). In contrast, Figure 13 (b) shows the interface after shear-slip failure, where the peak shear stresses of the two curves (NAC30-1-S and NAC30-2-S) differ even more, and the trajectories after the peak also differ more. This indicates that the differences in interface morphology are magnified after shear-slip. This dynamic change and randomness also make it more difficult to predict the aggregate interlock in concrete shear.

Overall, these observations indicate that concrete crack interfaces inherently possess asymmetry in roughness and shear performance, and asymmetry decreases after shear slip but does not disappear completely. Such interface differences directly influence aggregate interlocking, shear resistance, and the subsequent mechanical behavior of cracked concrete structures.

4. Analysis of aggregate interlock mechanism by simulation

4.1 Analysis of crack propagation and interface contact mechanisms

Based on the images provided showing the shear-slip behavior and crack propagation of different concrete types (NAC30, NAC60, RAC30, RAC60) under different shear-slip displacements (1 mm, 3 mm, 5 mm, and 7 mm), the analysis is as follows:

NAC30 (Figure 14 (a)) and RAC30 (Figure 14 (c)) exhibited no significant localized crack propagation at the interface under 1 mm shear slip. As displacement increased to 3 mm and 5 mm, crack propagation gradually penetrated deeper into the concrete matrix, reflecting aggregate interlocking and localized damage. At 7 mm displacement, a broad damage zone formed around the cracks, indicating severe damage leading to loss of aggregate interlocking and a significant reduction in shear strength. However, compared to NAC30, the interface damage in RAC30 was more uniformly distributed across the contact interface. This phenomenon is also illustrated in the subsequent three-dimensional images (Figure 15).

NAC60 (Figure 14 (b)) and RAC60 (Figure 14 (d)) exhibited no significant crack propagation at the interface during 1 mm and 3 mm shear slip, indicating high matrix strength and initial aggregate interlocking. When shear slip increased to 5 mm, insufficient interface contact led to localized failure. At 7 mm slip, damage zones appeared but were confined to peak contact areas, indicating enhanced crack control and internal interlocking due to increased matrix strength. Since both NAC60 and RAC60 exhibited aggregate fracture prior to shear slip, interfacial roughness decreased. Combined with the above factors, interfacial damage in NAC60 and RAC60 was less severe than in NAC30 and RAC30.

In Figure 15 (a) (approximately 1 mm slip) exhibits peak-valley contact; in Figure 15 (b) (approximately 7 mm slip) shows the crack propagation process following severe damage.

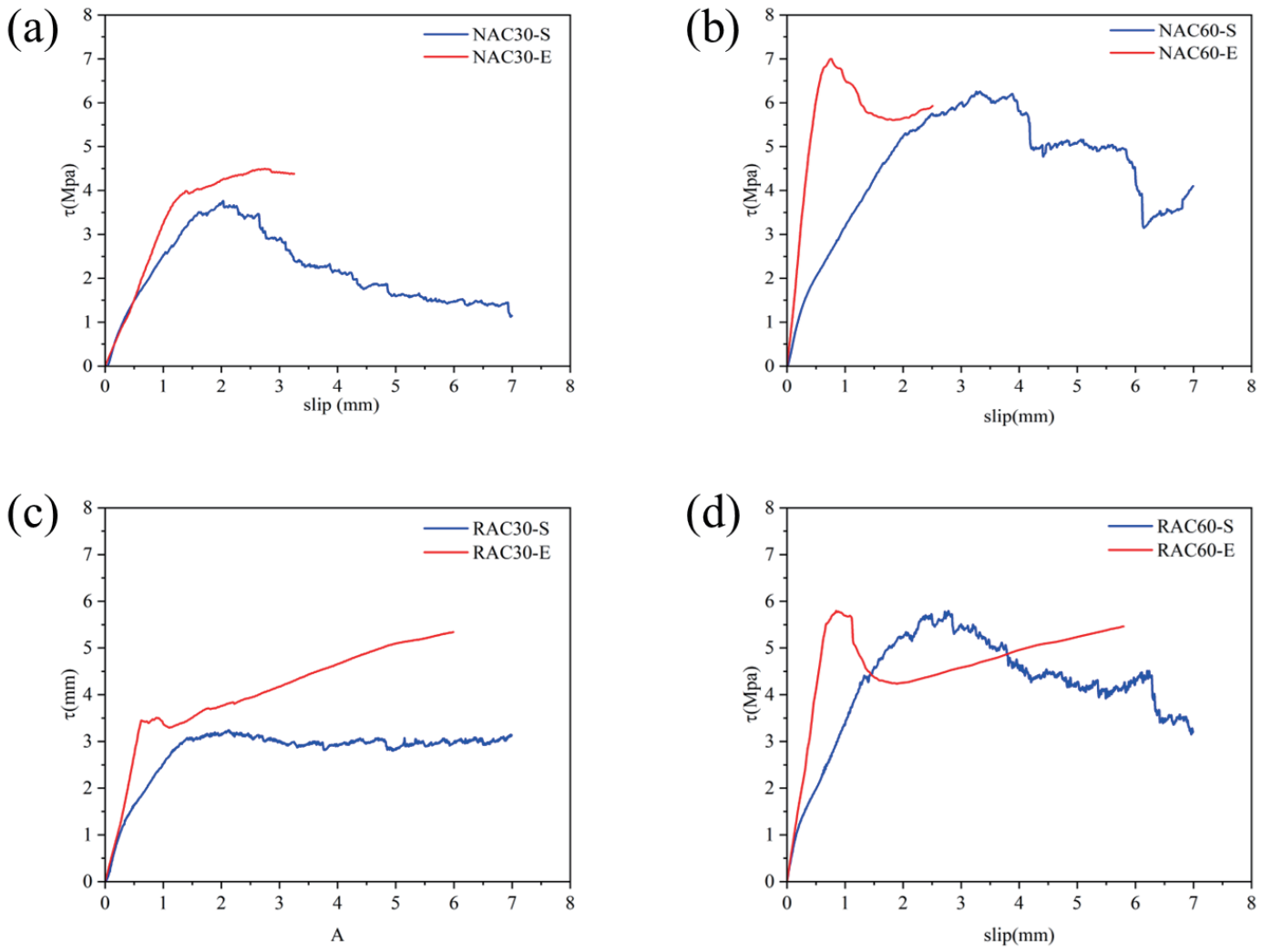

Figure 12 Comparison of DEM results with experimental results: (a) NAC30, (b) NAC60, (c) RAC30, and (d) RAC60 (NAC30-S: DEM results, NAC30-E: experiment results, and the others are the same.)

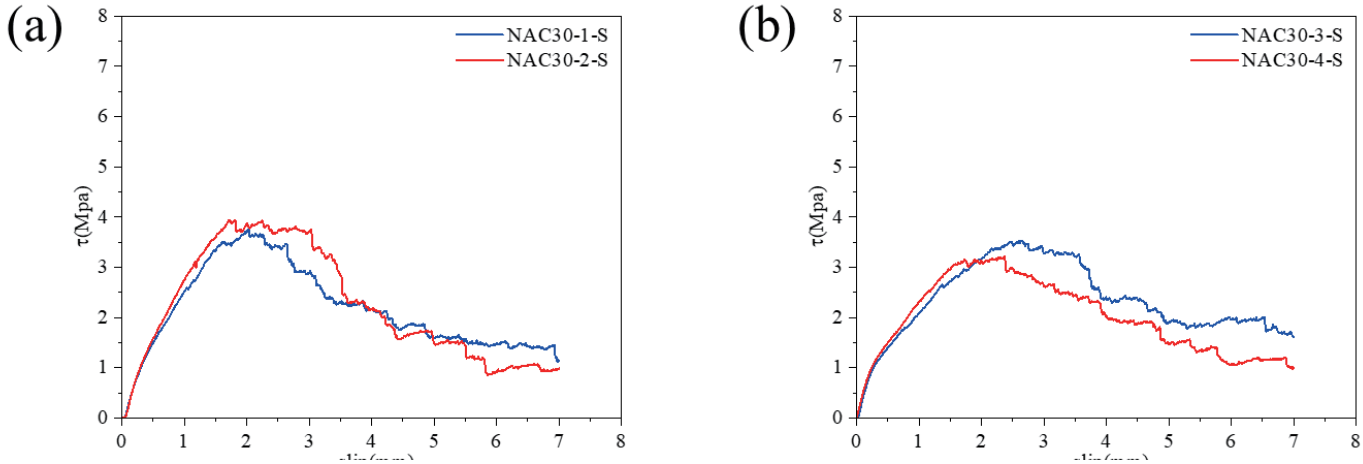

Figure 13 Comparison of DEM results on both sides of the same crack interface: (a) before shear-slip and (b) after shear-slip

The micro-mechanics of aggregate interlock involve not only peak-valley contact (high peak and valley) but also ordinary rough contact (low peak and valley). When a peak surface contacts a corresponding valley surface, the relative tangential displacement causes normal contact force, which correlates with the local surface inclination (roughness). Under external constraints in normal direction, this cannot induce expansion but generates a normal reaction force, further compressing the contacting particles. Crack propagation in the DEM involves local failure. In the bonded particle model, when the composite

stress index reaches its bearing limit, the interface particles or bonds fail. Contact particles at the crack interface displace and redefine the crack contact. During the damage and crack propagation phase, particle compression and spalling continuously slip and destroy the peak body. Bonding failure occurs between the top one or two particle layers, the contact zone flattens. This process appears as blue crack propagation and localized contact "gaps." Even after local crushing, numerous micro-contacts persist (smaller-scale interlock, manifested in the DEM model as re-contact of particles at the crack interface). As shown in Figure 15 (b), crack propagation zones appear in particles at the peak-valley contact interface. This occurs because the aggregate interlocking formed at the peak-valley interface induces stress concentration, leading to particle failure or localized slip differences.

Another key focus in concrete shear-slip studies is the stress distribution within the concrete. Conventional shear-slip tests typically employ digital speckle tracking to capture surface displacement and stress distribution, enabling analysis of crack propagation and kinematics. In the DEM result analysis, we can examine the impact of interface contact based on the location of fractures. As shown in Figure 16, The majority of interlock failure fractures occurred at the specimen's interface, with some fractures also present along the specimen's edges. The NAC30 interface exhibits larger geometric joint scales, while the RAC30 interface features smaller scales with richer texture variations. At the shear-slip of 3 mm, RAC30 had a higher number of fractures than NAC30. Ultimately, NAC30 fractures more frequently than RAC30. We can also correlate the density of localized cracks with the scale of peak-valley interlocking at interface.

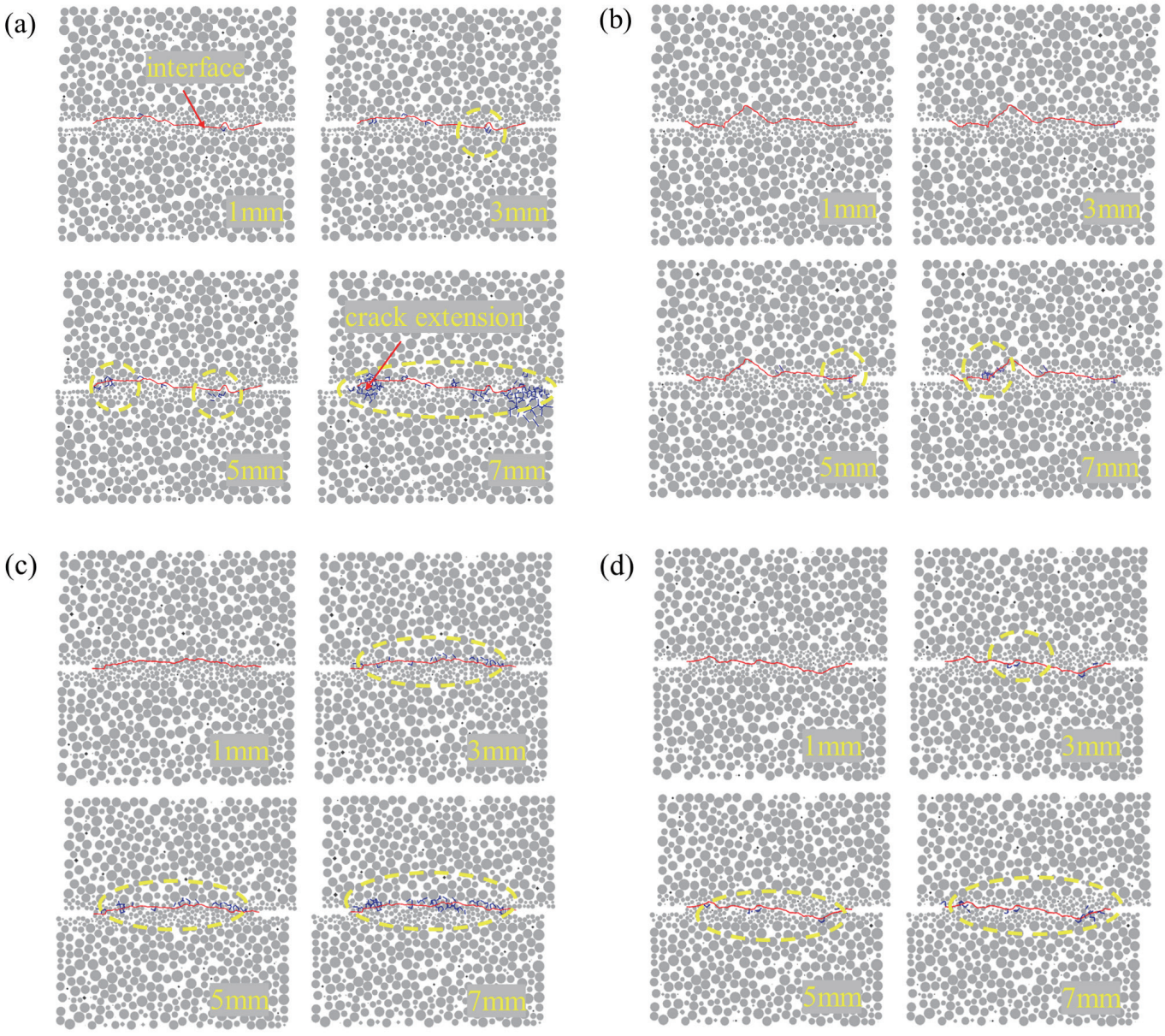

Figure 14 Comparison of DE results with different shear-slip displacements: (a) NAC30, (b) NAC60, (c) RAC30, and (d) RAC60

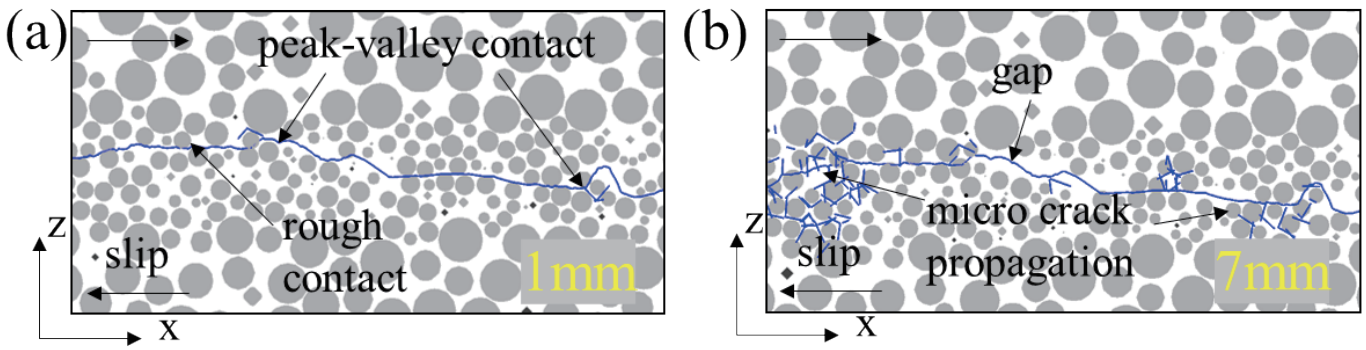

Figure 15 Fracture of particles in crack contact: (a) 1mm and (b) 7mm in x-x direction

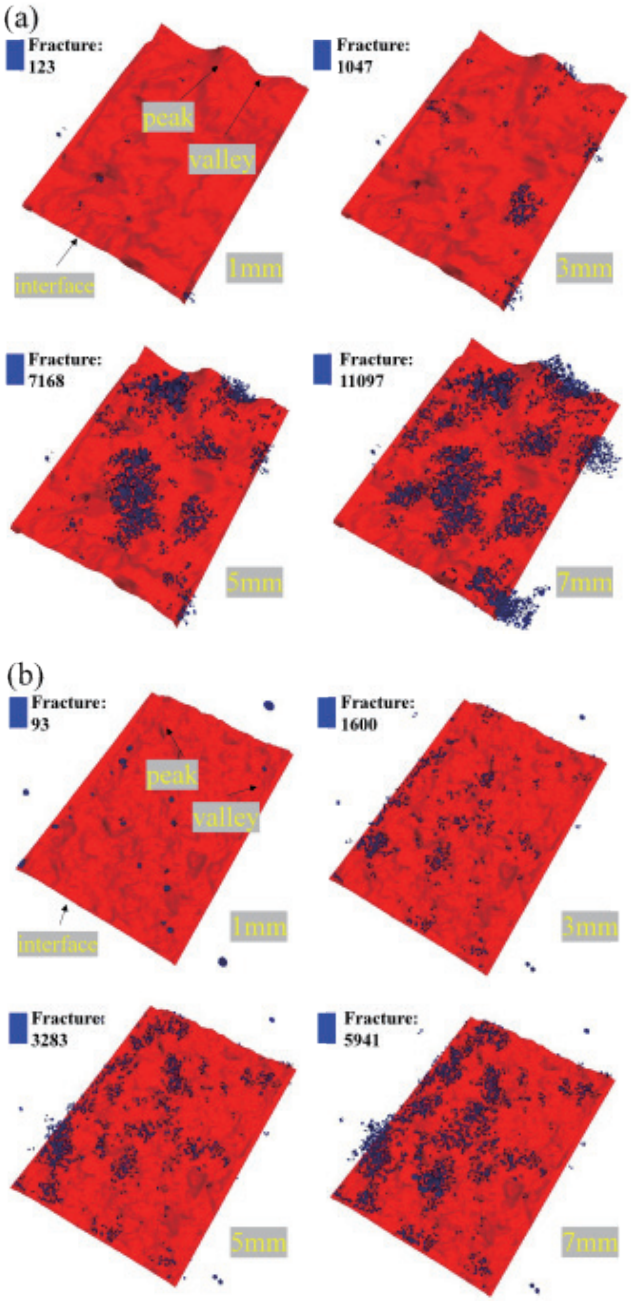

Figure 16 Comparison of DEM fractures with different interfaces: (a) NAC30 and (b) RAC30

4.2 Analysis of radial shear force distribution in DEM particles

The component of tangential force, ft that acts along the radial direction, nt is known as the radial shear force, frt , and it is used to describe the shear force distribution caused by the sheer-slip of the particles that occur at the actual rough interface between the cracks. The radial shear force distribution of the model particles is described in this paper. Schematic diagrams of particle radial contact forces are shown in Figure 17 [33] [34]. Based on radial shear forces and shear-slip curves, the study can analyze the contact force patterns dominant at different stages, as well as contact characteristics such as shear force distribution patterns, symmetry, and anisotropy. This enables an understanding of concrete behavior during shear-slip.

The tangential force generated at the particle interface can be decomposed into components relative to the local contact geometry. Specifically, the shear force is projected onto the radial direction, and the corresponding radial component at the contact point is determined according to the following expression:

$$fr\ t(ng)=fx\ t\cos\alpha+fx\ t\sin\alpha$$

Where, respectively, the tangential contact force components in the x and y axes are denoted by the symbols α and β. The contact point is defined as the angle of the azimuth (α) over the interval [0, 2π), whereas the polar angle (β) is covered by the range [0, π). To calculate the average radial shear force in the coordinate system, the sphere is separated into a 36 x 18 grid ($\Delta\alpha = 10^\circ$, $\Delta\beta = 10^\circ$).

Analysis of DEM typically differs somewhat from FEM. Since the DEM is based on discrete particles for simulation, each particle and the DEM itself are more abstract. For example: We define the contact between interface particles using real rough interfaces, but directly observing the profile composed of interface particles makes comparison and analysis difficult. Therefore, we typically use statistical analysis methods to collect and compare the states of relevant particles. Rose plots are a very common method for three-dimensional DEM, as the state of particles is based on multiple directions and angles. The mean values of all particle radial forces in the model were collected to analyze its applicability during the shear-slip process.

Based on the DEM curve (Figure 12), the shear-slip process

is divided into four stages: the initial elastic stage (0-1mm), the peak softening stage (1-3mm), the post-peak declining stage (3-5mm), and the smoothing stage (5-7mm). Statistical analysis and comparison of radial shear forces from simulation results of NAC30 were conducted as shown in Figure 18. During the initial elastic stage, particle contact angles were predominantly governed by multi-angle contact forces. This reflects the fact that in the DEM model, the close packing of particles results in contacts not being in the direction of shear-slip or in the vertical direction. As shear-slip increased, contact between particles at the interface deteriorated, with larger-angle contacts being disrupted. During the 5-7 mm slip stage, as the model's contact interface becomes smoother due to disruption, both small-angle (around 20 °) and large-angle (around 160 °) contacts increase on the interface. This local shear interface transformation can be reflected. In summary, contact plane angles during the shear-slip process are primarily distributed around 45°, 135°, 225°, and 315°. There are fewer contact angles near 90 ° and 270 ° (perpendicular to the slip direction), and similarly fewer contact angles near 0° and 180° (parallel to the slip direction). Although the contact interface is disrupted during shear-slip, most contact angles undergo slight changes as the interface contacts are reconfigured.

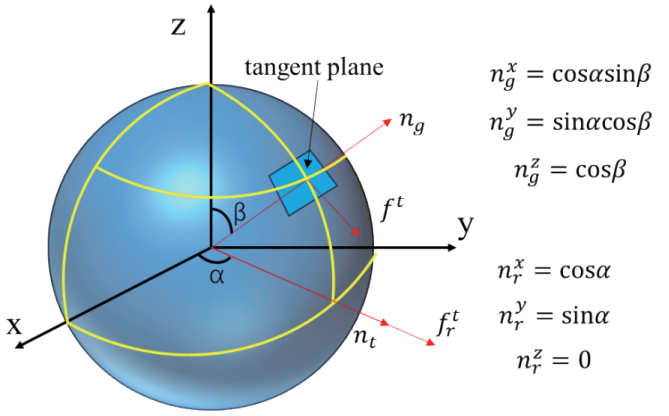

Figure 17 Definition of the radial tangential contact force

4.3 Analysis of contact orientation in DEM particles

The study analyzes the shear-slip mechanism through radial shear forces (Figure 18). Using a very similar approach, we collect the number of contacts between cracks of different directions (Figure 19). Note that the cracks referred to here are not primary crack interfaces, but rather particle cracks resulting from particle contact failure. The same applies to subsequent statements in this section. This method provides a more visual comparison of differences in particle failure under the coupling of factors such as different aggregates and concrete strength. The orientation of the three-dimensional rose diagrams in Figure 19 aligns with the coordinate axes shown. The column heights in these rose diagrams represent the contacts and contact force in that direction. This type of analysis is frequently employed in rock mechanics to characterize microcracks [35, 36, 37, 38]. When particle contact fractures occur in the DEM, microcracks are generated. The larger the column (red column) in the 3D rose diagram, the greater the crack contact for that orientation. The smaller the column (blue column), the lesser the crack contact for that orientation.

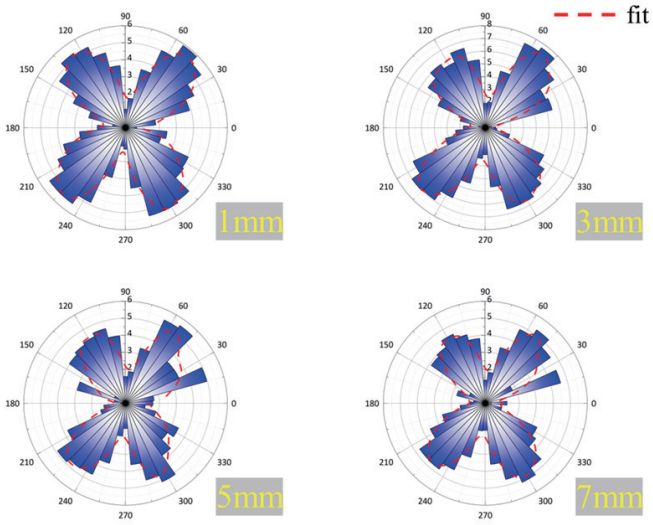

Figure 18 Radial shear force distribution at different slip values (Rose diagram 0° consistent with shear-slip direction, radial sear force unit: N)

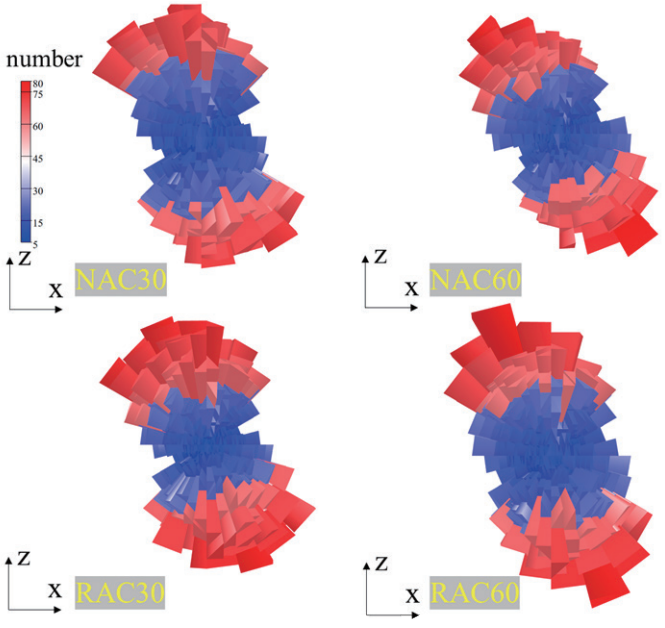

Figure 19 Orientation distribution of contacting planes at the slip of 7 mm (three-dimensional rose diagram's x-direction consistent with shear-slip direction)

Figure 19 compares the crack count and orientation distribution based on the particle model. The primary orientation distributions of contacting planes in NAC30, NAC60, RAC30, and RAC60 are broadly similar and exhibit symmetrical characteristics. However, we also note differences in the number and distribution of interface failure cracks defined by different true rough interface models. As NAC strength

increases, the symmetry and angular distribution of the three-dimensional rose diagram shift, becoming more biased toward the x-x direction. This occurs because higher NAC strength reduces interface roughness by inducing greater aggregate fracture during pre-cracking (before shear-slip). Under these conditions, the crack orientation distribution in the DEM reflects distinct interface evolution and changes. Comparing NAC and RAC results, since RAC exhibits lower interface roughness and matrix strength than NAC at equivalent strength, RAC shows a greater number of cracks surrounding in the z-z direction angle compared to NAC. Moreover, the direction of these cracks is mostly developed vertically into the matrix on both sides of the interface. This indicates that at equivalent strength, RAC demonstrates weaker resistance than NAC, consequently producing more cracks. This is consistent with the general experimental phenomena and analysis. Notably, RAC60 exhibits an exceptionally high number of individual angles (Figure 19). This phenomenon aligns with roughness investigations, where shear-slip increases the original interface' s roughness parameters. In summary, the results of three-dimensional crack contact are similar to the conclusions regarding the radial force distribution of particles mentioned above. During shear slip, contact angles primarily distributed around 45 ° on different planes (such as near 135 ° and 315 °). However, contact angles also existed near 90 ° and 270° (perpendicular to the slip direction) for this crack contact. This demonstrates that new displacements or deformations occurred in the contact between crack particles relative to the initial model particle contact, generating new-angle particle-crack contacts.

5. Conclusion

This study systematically investigated the shear–slip behavior of cracked concrete interfaces by combining high-resolution interface geometry acquisition with a discrete element modeling framework. The analytical model proposed in this study innovatively incorporates realistic interface geometries derived from high-resolution surface scans into a discrete element framework, enabling accurate representation of aggregate interlock and shear-slip mechanisms in cracked concrete interfaces at a small scale less than millimeter order (mesoscale). Its predictive capability has been validated through multiple experimental tests, including natural aggregate concrete (NAC) and recycled aggregate concrete (RAC) specimens, parametric numerical simulations covering the range of concrete strengths and aggregate types, and the analyses of interface roughness parameters. The key findings are as follows:

The DEM simulation results disclose the effects of concrete strength and aggregate type as follows. Concrete strength significantly affects aggregate interlock performance. Higher-strength concrete (NAC60) exhibits greater peak shear strength and superior shear resistance than lower-strength concrete (NAC30). This improvement is attributed to stronger aggregate-matrix bonding and reduced micro-cracking at lower shear-slip displacements, allowing high-strength concrete to maintain interlock integrity for longer periods.

Concrete type substantially influences interlocking behavior. Natural concrete consistently demonstrates higher peak shear strengths and more pronounced post-peak responses compared to recycled concrete. In contrast, RAC shows earlier crack initiation, lower peak shear strengths, and smoother post-peak shear-slip curves, primarily due to early fracture and weaker bonding of recycled aggregates.

The DEM simulation effectively captures the complex aggregate interlock mechanism and shear-slip behavior of concrete interfaces at the mesoscale. DEM simulations closely replicate the observed aggregate damage and crack propagation patterns from experimental data, although peak shear stresses are slightly underestimated. The DEM approach provides a valuable tool for analyzing detailed shear mechanisms in cracked concrete structures. Although DEM to some extent reflects the differences between natural aggregates and recycled aggregates, it relies on simplified methods to a certain degree. This aspect still requires some degree of improvement.

The DEM results reveal that peak-valley interlock dominates the early shear-slip response by mobilizing normal reaction forces through peak-valley contact and rough surface contact. With increasing slip, bond breakage and particle spalling flatten the interface, yet residual micro-contacts sustain smaller-scale interlock. Stress concentration at peak–valley contacts drive localized crack propagation and heterogeneous particle displacements, while the redistribution of stresses in shear slip and normal directions reflects the transition from dispersed states to shear-interface concentration, consistent with observed shear-swelling and spalling. Statistical analysis further shows that contact orientations reconfigure toward dominant shear directions, supporting the division of the shear–slip process into four characteristic stages. These findings confirm the multi-scale nature of aggregate interlock and its governing role in the progressive evolution of concrete shear failure.

The DEM analysis reveals that particle contact evolution during shear slip follows clear directional and mechanical patterns. Radial force and crack-orientation statistics consistently show that despite progressive interface disruption, particle contacts predominantly cluster around oblique angles ($\approx 45°, 135°, 225°, 315°$), while contacts parallel or perpendicular to the slip direction remain limited. Increasing shear slip smooths the interface, reconfiguring contacts and generating new microcracks with expanded angular ranges.

Future research

Future research should primarily focus on improving the DEM framework and expanding its applicability to shear–slip analysis of concrete interfaces. First, potential enhancements to the DEM model include incorporating more realistic contact constitutive laws, employing advanced bond and cohesive interaction models, and introducing particle breakage mechanisms to better capture local damage evolution and aggregate fragmentation. These improvements would enable a more faithful representation of the mechanical

response of rough interfaces. Second, larger-scale shear–slip simulations should be explored to investigate size effects, structural relevance, and the transition from particle-scale interactions to macroscopic shear mechanisms. Such studies would help clarify how aggregate interlock evolves across different geometric and loading scales. Third, future work may consider coupling DEM with continuum-based methods or multi-scale modeling approaches to achieve a more comprehensive description of shear behavior, integrating microscopic interlocking processes with macroscopic constitutive responses. Through these advancements, DEM has the potential to offer deeper insights into the mechanisms governing concrete interface shear resistance and provide stronger theoretical support for structural design and analysis.

Authorship contribution statement

Zhuofan GU: Writing – original draft, Investigation, Data curation, Formal analysis, Methodology.

Jiehui WANG: Writing – review & editing, Supervision.

Li WANG: Writing – review & editing.

Tamon UEDA: Writing – review & editing, Supervision, Project administration, Funding acquisition.

Declaration of competing interest

The authors declare that they have no known competing financial interests or personal relationships that could have appeared to influence the work reported in this paper.

Acknowledgements

The research was supported by the NSFC Funding "Creative study on integrated approach for life cycle management of concrete structures and assessment for Net-Zero" (Project code: W2531041). The authors would like to thank Prof. Yuxi ZHAO of Zhejiang University for his valuable suggestions at the initial stage of this study. The staff of the College of Civil and Transportation Engineering, Shenzhen University and Guangdong Provincial Key Laboratory of Durability for Marine Civil Engineering are acknowledged for their help in the experimental development process. The authors also thank the support from the Shenzhen Key Laboratory for Low-Carbon Construction Material and Technology, Shenzhen University.

Data availability statement

The data that support the findings of this study are available from the corresponding author upon request.

Reference

[1] HER, N. (1970). "Theory and Experiments on the Mechanical Behaviour of Cracks in Plain and Reinforced Concrete Subjected to Shear Loading". Publications in HERON since.

[2] Cavagnis, F., Ruiz, M. F., & Muttoni, A. (2018). "A Mechanical Model for Failures in Shear of Members without Transverse Reinforcement Based on Development of a Critical Shear Crack". Engineering Structures, 157, 300-315.

[3] Li, B., Maekawa, K., & Okamura, H. (1987). Contact density model for cracks in concrete. In IABSE colloquium, Delft. 1987, 1: 51-62.

[4] BUJADHAM, B., & MAEKAWA, K. (1992). "Qualitative Studies on Mechanisms of Stress Transfer across Cracks in Concrete". Doboku Gakkai Ronbunshu, 1992(451), 265-275.

[5] Jayasinghe, T., Gunawardena, T., & Mendis, P. (2022). "Aggregate Interlock in Fractured Concrete Mesoscale Models: A Novel Finite Element Modelling Approach". Archives of Civil and Mechanical Engineering, 22(4), 165.

[6] López, C. M., Carol, I., & Aguado, A. (2008). "Meso-Structural Study of Concrete Fracture Using Interface Elements". I: Numerical Model and Tensile Behavior. Materials and Structures, 41(3), 583-599.

[7] Wang, X. (2015). "Computational technology for damage and failure analysis of quasi-brittle materials" (Doctoral dissertation, University of Manchester).

[8] Wang, W., & Lin, J. (2022). "Study on Steel-Concrete Composite Structure Push-out Tests Considering the Interfacial Slip Behavior". 2022 8th International Conference on Hydraulic and Civil Engineering: Deep Space Intelligent Development and Utilization Forum (ICHCE)

[9] Potyondy, D. (2002). "A Bonded-Disk Model for Rock: Relating Microproperties and Macroproperties". In Discrete Element Methods: Numerical Modeling of Discontinua (pp. 340-345).

[10] Potyondy, D. O. (2006). "The Effects of Void Shape on the Mechanical Properties of Rock". Yucca Mountain Project, Las Vegas, NV (United States).

[11] Zhou, M., He, X., Wang, H., Wu, C., & Wei, B. (2025). "Mesoscale discrete analysis of mechanical properties of steel fiber reinforced concrete. Journal of Building Engineering", 105, 112437.

[12] Zhou, M., He, X., Wang, H., Wu, C., & He, J. (2023). "Mesoscale Modeling of Polypropylene Fiber Reinforced Concrete under Split Tension Using Discrete Element Method". Construction and Building Materials, 404, 133274.

[13] Nitka, M., & Tejchman, J. (2020). "Meso-Mechanical Modelling of Damage in Concrete Using Discrete Element Method with Porous Itzs of Defined Width around Aggregates". Engineering Fracture Mechanics, 231, 107029.

[14] Wang, P., Gao, N., Ji, K., Stewart, L., & Arson, C. (2020). "Dem Analysis on the Role of Aggregates on Concrete Strength". Computers and Geotechnics, 119, 103290

[15] Yang, L., Li, K., Hu, X., Peng, Z., Liu, Q.-f., & Shi, C. (2024). "Mesoscopic Discrete Modeling of Compression and Fracture Behavior of Concrete: Effects of Aggregate Size Distribution and Interface Transition Zone". Cement and Concrete Composites, 147, 105411.

[16] Su, H., Li, H., Hu, B., & Yang, J. (2021). "A Research on the Macroscopic and Mesoscopic Parameters of Concrete Based on an Experimental Design Method". Materials, 14(7), 1627.

[17] Bazant, Z. P., & Gambarova, P. (1980). "Rough Cracks in Reinforced Concrete". Journal of the Structural Division, 106(4), 819-842.

[18] Paulay, T., & Loeber, P. (1974). "Shear Transfer by Aggregate Interlock". Special Publication, 42, 1-16.

[19] Potyondy, D. (2011). "Parallel-Bond Refinements to Match Macroproperties of Hard Rock". Continuum and distinct element numerical modeling in geomechanics, 459-465.

[20] Holt, R., Kjølaas, J., Larsen, I., Li, L., Pillitteri, A. G., &

Sønstebø, E. (2005). "Comparison between Controlled Laboratory Experiments and Discrete Particle Simulations of the Mechanical Behaviour of Rock". International journal of rock mechanics and mining sciences, 42(7-8), 985-995.

[21] Potyondy, D. O. (2015). "The Bonded-Particle Model as a Tool for Rock Mechanics Research and Application: Current Trends and Future Directions". Geosystem Engineering, 18(1), 1-28.

[22] Potyondy, D. O., & Cundall, P. A. (2004). "A Bonded-Particle Model for Rock. International journal of rock mechanics and mining sciences", 41(8), 1329-1364.

[23] Ivars[1], D. M., Potyondy, D. O., Pierce, M., & Cundall, P. A. (2008). "The Smooth-Joint Contact Model".

[24] Pierce, M., Cundall, P., Potyondy, D., & Ivars, D. M. (2007). "A synthetic rock mass model for jointed rock". In ARMA Canada-US Rock Mechanics Symposium (pp. ARMA-07). ARMA.

[25] Nitka, M., & Rucka, M. (2025). "3d Dem Modelling of Acoustic Emission in Concrete: Insights into Elastic Waves Initiated by Microcracks". Ultrasonics, 150, 107599.

[26] Zhou, M., He, X., Wang, H., Wu, C., Wei, B., & Li, Y. (2024). "3d Mesoscale Discrete Element Modeling of Hybrid Fiber-Reinforced Concrete". Construction and Building Materials, 447, 138006.

[27] Yu, J.-C., Wang, J.-T., Pan, J.-W., Guo, N., & Zhang, C.-H. (2023). "A Dynamic Fem-Dem Multiscale Modeling Approach for Concrete Structures". Engineering Fracture Mechanics, 278, 109031.

[28] Zhao, H., Zhou, A., Zhang, L., & Arulrajah, A. (2025). "A Novel Three-Dimensional Dem Model for Recycled Aggregate Concrete Considering Material Heterogeneity and Microcrack Evolution". Composite Structures, 352, 118677.

[29] Zhao, H., & Zhou, A. (2024). "Effects of Recycled Aggregates on Mechanical and Fractural Properties of Concrete: Insights from Dem Modelling". Composites Part A: Applied Science and Manufacturing, 186, 108395.

[30] Zhang, S., Liu, F., Ying, M., & Zeng, W. (2024). "Experimental and Dem Analysis for the Shear Characteristics of Interface between Sand and Irregular Concrete under Dynamic Normal Loading". Computers and Geotechnics, 173, 106514.

[31] Nitka, M., & Tejchman, J. (2024). "Mesoscopic simulations of a fracture process in reinforced concrete beam in bending using a 2D coupled DEM/micro-CT approach". Engineering Fracture Mechanics, 304, 110153.

[32] Ouafdel, H., Wood, D. M., & Belkheir, K. (2000). "Numerical simulations of granular assemblies with three-dimensional ellipsoid-shaped particles". University of Waterloo.

[33] Li, B., Song, X., Fu, J., Yang, M., Ti, Y., & Ding, Q. (2025). "Investigations on texture and shear resistance characteristics of LUHPC first-time interlayer roughening: Experiment and numerical studies". Construction and Building Materials, 492, 142943.

[34] Fan, D. D., Zhang, T., Yu, L. Y., Hu, L. H., Su, H. J., & Wei, J. B. (2023). "A numerical study based on GBM3D-DEM model: Multi-level force chain analysis in dynamic flexural tensile strength test". Journal of Central South University, 30(11), 3821-3839.

[35] Peng, Y., Zhang, T., Yu, L., Li, J., Gao, Y., & Tian, W. (2023). "Numerical investigation on the effect of intergranular contact bonding strength on the mechanical properties of granite using PFC3D‐GBM". International Journal for Numerical and Analytical Methods in Geomechanics, 47(5), 694-716.

[36] Zhang, T., Yu, L., Peng, Y., Ju, M., Yin, Q., Wei, J., & Jia, S. (2022). "Influence of grain size and basic element size on rock mechanical characteristics: insights from grain-based numerical analysis". Bulletin of Engineering Geology and the Environment, 81(9), 347.

[37] Wang, Z., Yang, S., Li, L., Tang, Y., & Xu, G. (2021). "A 3D Voronoi clump based model for simulating failure behavior of brittle rock". Engineering Fracture Mechanics, 248, 107720.

[38] Yang, L., Shi, Z., Li, K., Hu, X., & Shi, C. (2025). Expansion of irregularly shaped aggregate induced by alkali-silica reaction: Insights from numerical modeling. Cement and Concrete Research, 187, 107727.

[39] Huang, P., Pan, X., Niu, Y., & Du, L. (2022). Concrete failure simulation method based on discrete element method. Engineering Failure Analysis, 139, 106505.